SLANTED-RAY MULTIPLE REFLECTIONS (1-1/2-D)

[based on SEP-7, p. 1-14, and SEP-12]

If the earth were purely stratified all countries would have an equal proportion of oil but we would all be under 2-3 kilometers of sea water. To escape from such purely stratified mathematical models we will retain flat horizontal layers of constant velocity but allow the reflectivity of the interfaces between them to vary laterally in strength. The lateral change will be taken to be slow compared to a wavelength but noticeably large within the geophone spread. The seafloor reflection is especially liable to have such reflectivity variations. Such irregularities could result from recent meanders and bars of deltaic deposition, as in the Gulf coast, or recent channel erosion and refill, as is common on the West Coast. Even though the seafloor may now be quite flat, it is very common to observe "statics" and variation in reflection strength. Mathematically we will characterize our present approach as one which is valid for ***large*** offsets (say at 45-degree angles) but for ***small*** earth dips (say to 5 degrees). In this geometry a simple seafloor multiple can hit the seafloor at two locations which are widely enough separated that the two depths could differ by more than a seismic wavelength. So being more general than one dimension but not so general as two, this study could be called "multiples in 1-1/2 dimensions."

A Slanted-Incidence Ray Theory

Equation (6) of the previous lecture was developed with the idea that everything was independent of the horizontal x-axis. But it would seem valid to allow for some slow variation in the horizontal direction merely by attaching a superscript x to each of the functions in (6). In order to allow lateral variation within the geometry under consideration we redraw figure 1 in "Time-Series and One-Dimensional Multiple Reflection" as figure 1 here, where for purposes of simplification we have taken the line of constant x to be along the slanted ray of the ***upcoming*** wave. The appropriate extension of equation (6) in view of the geometry of figure 1 is

$$u_3^x = c_1^x d_2^{x-1} + c_2^x d_1^{x-2} + c_3^x d_0^{x-3} \qquad (1)$$

or

$$u_t^x = \sum_{z=1}^{t} c_z^x d_{t-z}^{x-z} \qquad (2)$$

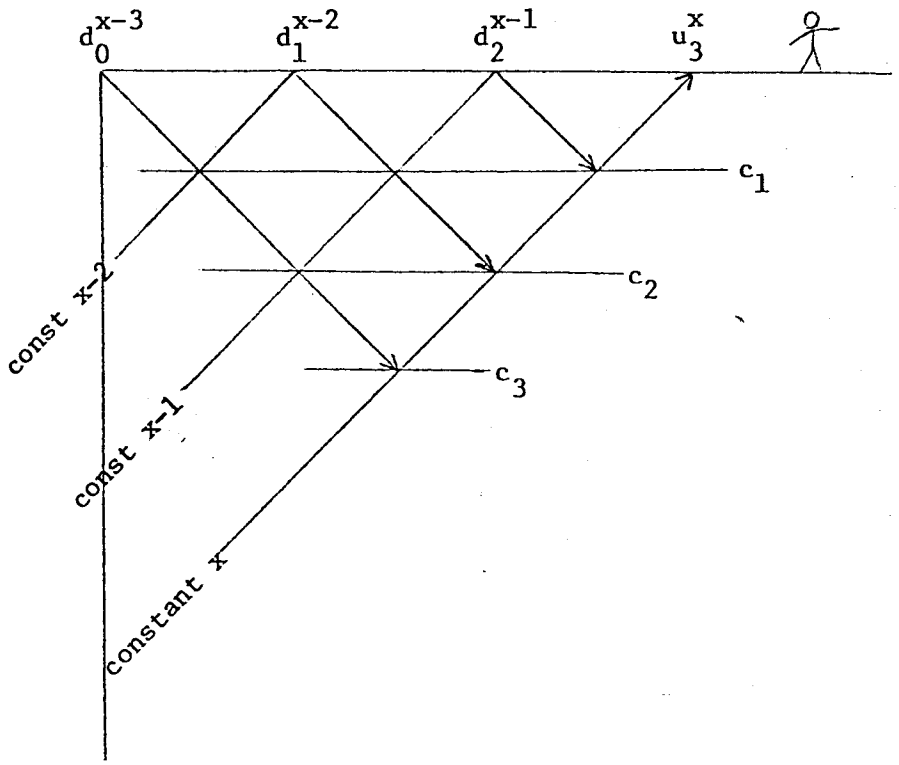

FIG. 1. Geometry for multiple reflection where reflection coefficients may vary in the horizontal x-direction.

The Z-transform method which works for vertical incidence does not appear to work for slanted problems. Nonetheless, it is a straightforward matter to show how we may recursively solve forward and inverse problems. Suppose the source waveform s_t^x is a constant function of x and an impulse function of

time at t = 0. Then at times greater than zero, equation (2) is

$$-d_t^x = \sum_{z=1}^{t} c_z^x \, d_{t-z}^{x-z} \tag{3}$$

Separate out from the sum the term at z = t, namely $c_t^x \, d_0^{x-t}$. At zero time there is no upcoming wave so the downgoing wave equals the source function. The negative of (3) now becomes

$$d_t^x = -c_t^x - \sum_{z=1}^{t-1} c_z^x \, d_{t-z}^{x-z} \tag{4}$$

Equation (4) may be used recursively for forward modeling since all of the values of d on the right side are earlier than (***and*** laterally shifted from) the value of d being computed on the left side. Although we have no Z-transform theory for stability, experience has shown that everything seems to behave as in the vertical-incidence case.

Inversion

For the inverse problem we merely rearrange the terms of (4) to get

$$c_t^x = -d_t^x - \sum_{z=1}^{t-1} c_z^x \, d_{t-z}^{x-z} \tag{5}$$

We notice that the values of c on the right side of (5) are all earlier (or above) the value of c being computed on the left. Values of c_t^x may be computed for all x and increasing t ("downward continuation") or for all t at increasing x ("roll along").

Use and Limitations of the Slanted Wave Theory

The first test of the modeling theory of equation (5) is to verify that on a simple model such as the one shown in figure 2a the appropriate multiples and peg-legs are present with the correct strength. The second test is to confirm that (5) does indeed suppress all the synthetic multiple reflections.

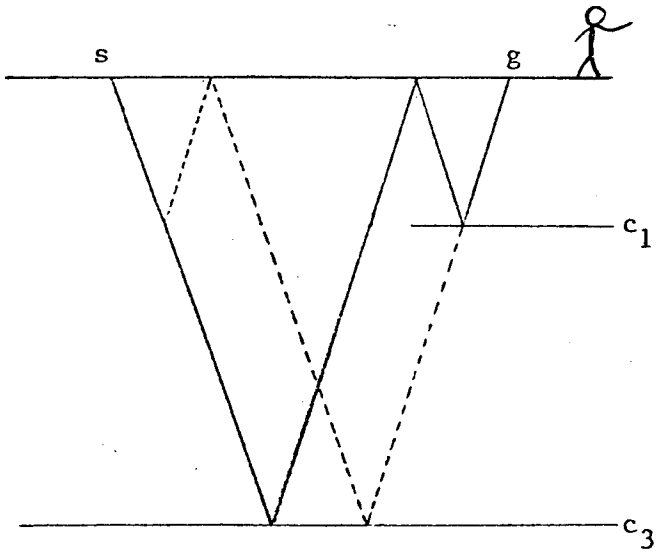

FIG. 2a. Peg-leg raypath (solid line) and missing peg-leg raypath (dashed line) in terminating reflector geometry.

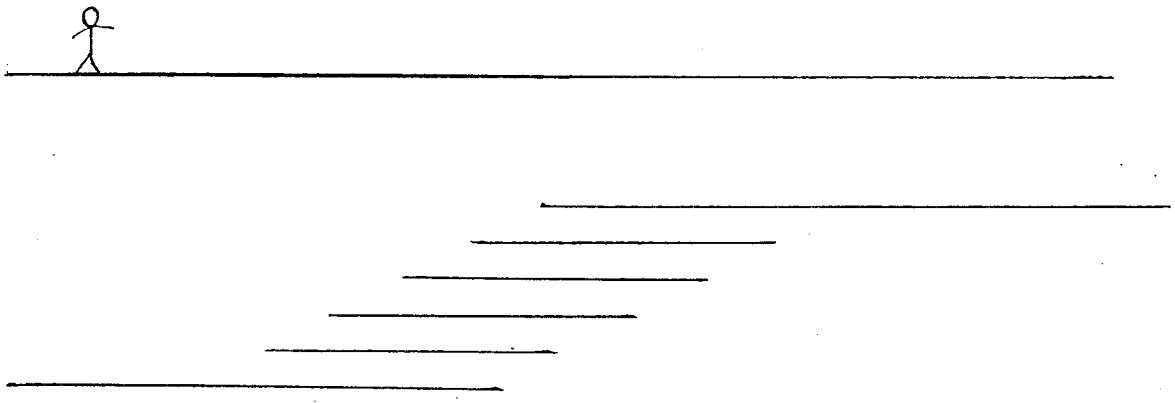

FIG. 2b. An appropriate arrangement of terminating reflectors gives the low-frequency behavior of a dipping bed.

In practice, of course, we will imagine a thousand or so layers, one at each sample interval on the time axis. Appropriate positioning of truncated reflectors can give the appearance of a dipping bed as shown in figure 2b. At low frequencies this model is indistinguishable from a dipping bed. A more realistic concern than the geometry of figure 2a is a dipping or curved seafloor. Both peg-leg reflections will then be present, but they may arrive at significantly different traveltimes. This adds a new ingredient to existing multiple prediction procedures. One property of a dipping seafloor is that the angle (from vertical) of an incident wave differs from the angle of the reflected wave. It turns out that (4) cannot model this angle change. Anticipating the results of multiple pages of wave-equation analysis, it can be said that equation (4) has utility for wide shot-to-geophone angles but only for small (5-degree) earth dip angles. Larger earth dip angles will eventually be incorporated by including diffraction terms such as ∂^t_{xx}, which arise in migration theory.

Synthetic Examples of 1-1/2-Dimensional Multiple Reflection

Figure 3a shows a model of a dipping, undulating sea bottom overlying a faulted reflector. Because of the small dip approximation, this model is valid only if we assume the plot has a large vertical exaggeration. Figures 3b and 3c show the vertical and slant seismograms, respectively. The first arrivals are labeled P_1 and P_2, the sea bottom multiples M_1 and M_2, and the corresponding peg-leg reflections PL_1 and PL_2.

An interesting effect can be noticed on the peg-legs. Usually it is assumed that different peg-leg paths of a given order produce a single arrival in the seismogram. Riley and Claerbout's (1976) theory predicted a modest splitting of the paths into different arrivals due to differences in their migration patterns. Figure 3c, however, shows widely separated arrivals for each multiple path. This happens because of the wide range of depths available for the seafloor bounce.

Actually equation (4) was not used directly for calculating figure 3. The x-z superscript was replaced by $x - 2z \tan \theta$ where Δx was considerably larger than Δz as is customary in field geometries. Then linear interpolation was done on the lateral coordinate.

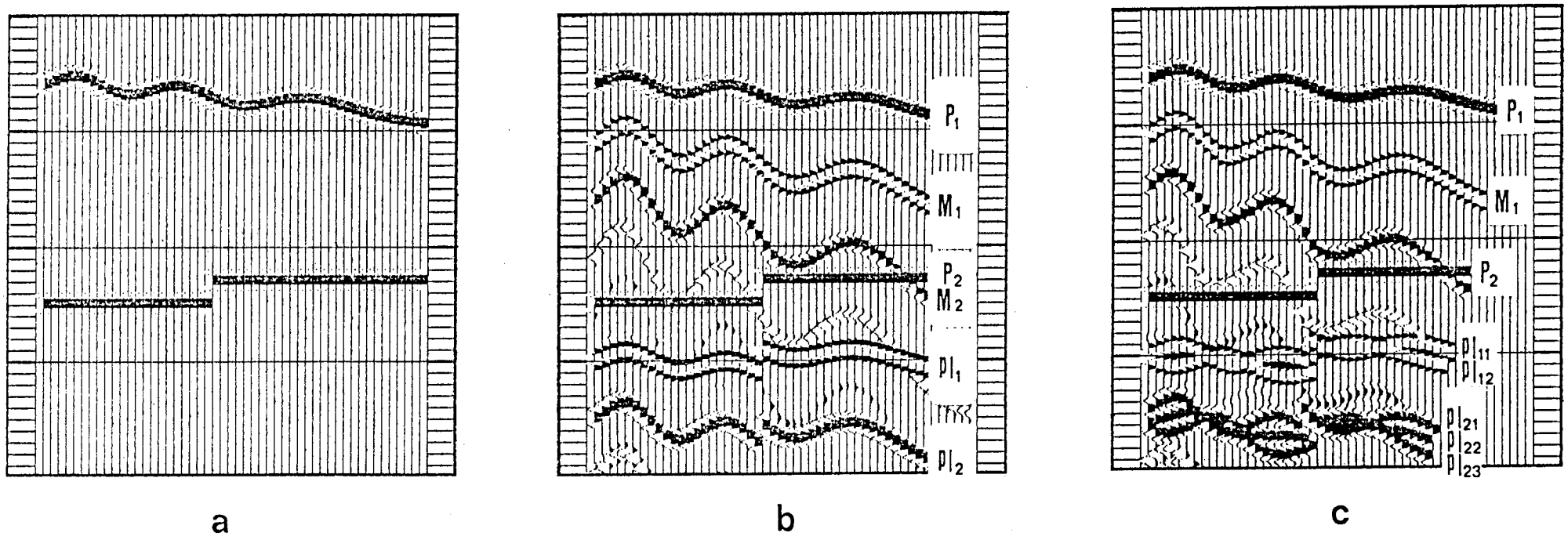

FIG. 3. Reflection seismogram for a dipping, undulating sea bottom. Figure (a) shows the original model of a dipping sea bottom overlying a faulted structure. (b) corresponds to the vertical seismogram showing, as before, the primary (P_1,P_2), multiple (M_1,M_2), and peg-leg (PL_1,PL_2) reflections. Figure (c) is the corresponding slanted seismogram. Besides subtle changes in the multiple reflections (shapes and arrival times), each peg-leg trajectory separates, that is, the first order peg-leg splits into two different arrivals (PL_{11} and PL_{12}) and the second order peg-leg into three different arrivals (PL_{21},PL_{22} and PL_{23}) .

Preparation of Field Data for Snell-Wave Inversion

The preparation of synthetic Snell waves by superposition of field data involves approximation of integration over an infinite range by summation over the recording cable. Errors of truncation and spatial aliasing are considered elsewhere. The deeper question of whether better practical results can be expected by mapping field data into Snell space or mapping Snell theory into data space is not considered at all. We merely consider what operations must be done to conventional field data to allow the processing equation (5) to be applicable.

Examination of figure 1 suggests that after selecting the numerical value of the Snell parameter p we mainly want to rid our field data of energy at all other Snell parameters. Slant stack will take survey line data P(s,g,t), which is a function of shot location s, geophone location g, and traveltime t, and contract out the shot dimension leaving a synthesized upcoming wave U(g,t). The process is quite confusing because there are three different kinds of time:

t = traveltime in the point source field experiments.

t' = $t - p(g - s)$ is interpretation time. The shallowest reflectors are seen just after $t' = 0$.

t_{pseudo} = time in the Snell pseudo-experiment of a moving source.

Time in the pseudo-experiment in a horizontally layered earth has the peculiar characteristic that the further you move down the geophone axis, the later the echoes will arrive. So we transform directly from the field-experiment time t to interpretation time t' by

$$t' = t_{pseudo} - px = t - p(g - s)$$

Figure 1 gives the correct impression that we ultimately plan to sample the depth axis at the same density as the time axis but gives the wrong impression in the sense that we do not necessarily intend to choose p to be equal to the ratio $\Delta t/\Delta g$ of the mesh sizes. To clarify this, figure 1 is

redrawn as figure 4. Figure 5 goes along with figure 4. It illustrates the superposition of shots required to make a pseudo-Snell wave. In figure 4 the discretization of the geophone axis is explicitly indicated, whereas figure 5 depicts a continuum on the shot axis. The lateral offset of B from C should be identical in figure 4 with both places in figure 5, but the slopes may differ because the vertical axes - z, t, and t', respectively - are not the same. A different chapter of these lectures shows how the medium velocity may be determined by measurement of the slope dt'/dg. After firing the Snell wave (summing over s at constant t') a short decaying exponential wavelet is seen on each of the arrivals. A seismic section for input to equation (5) consists of many side-by-side traces like the one shown as g_{1000}.

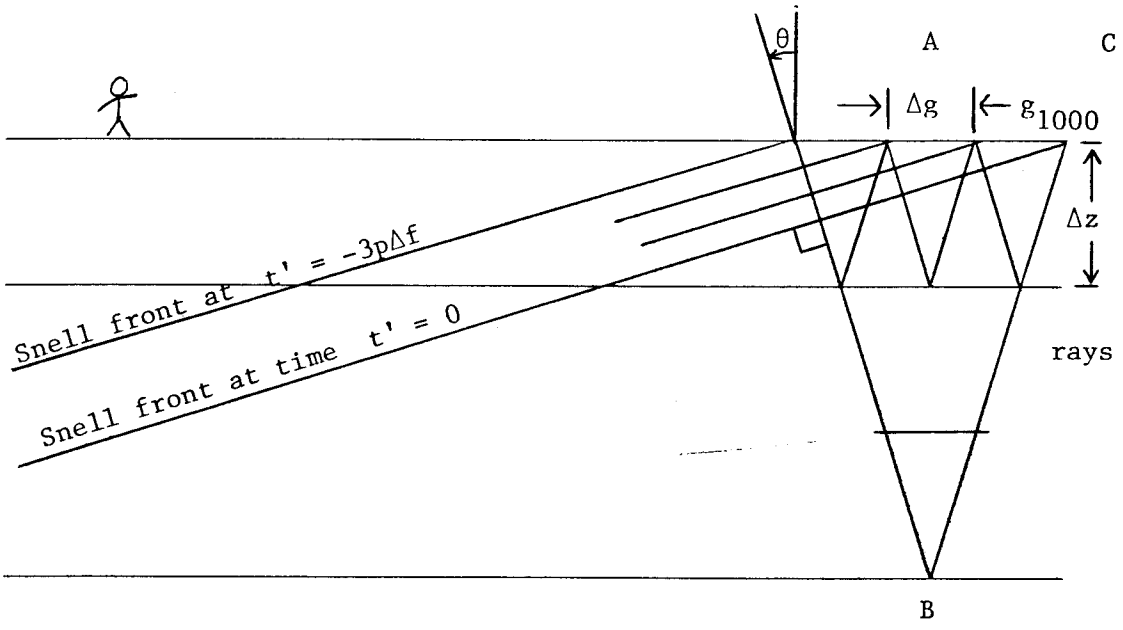

FIG. 4. Rays and fronts of Snell waves. Line BC is the upgoing path to the recorder g_{1000}.

Full Interpretation Coordinates

The variable t' has been referred to as an interpretation coordinate because shallow reflectors are seen just after t'=0, and horizontal beds give echoes which arrive without horizontal stepout, unlike the pseudo-Snell wave.

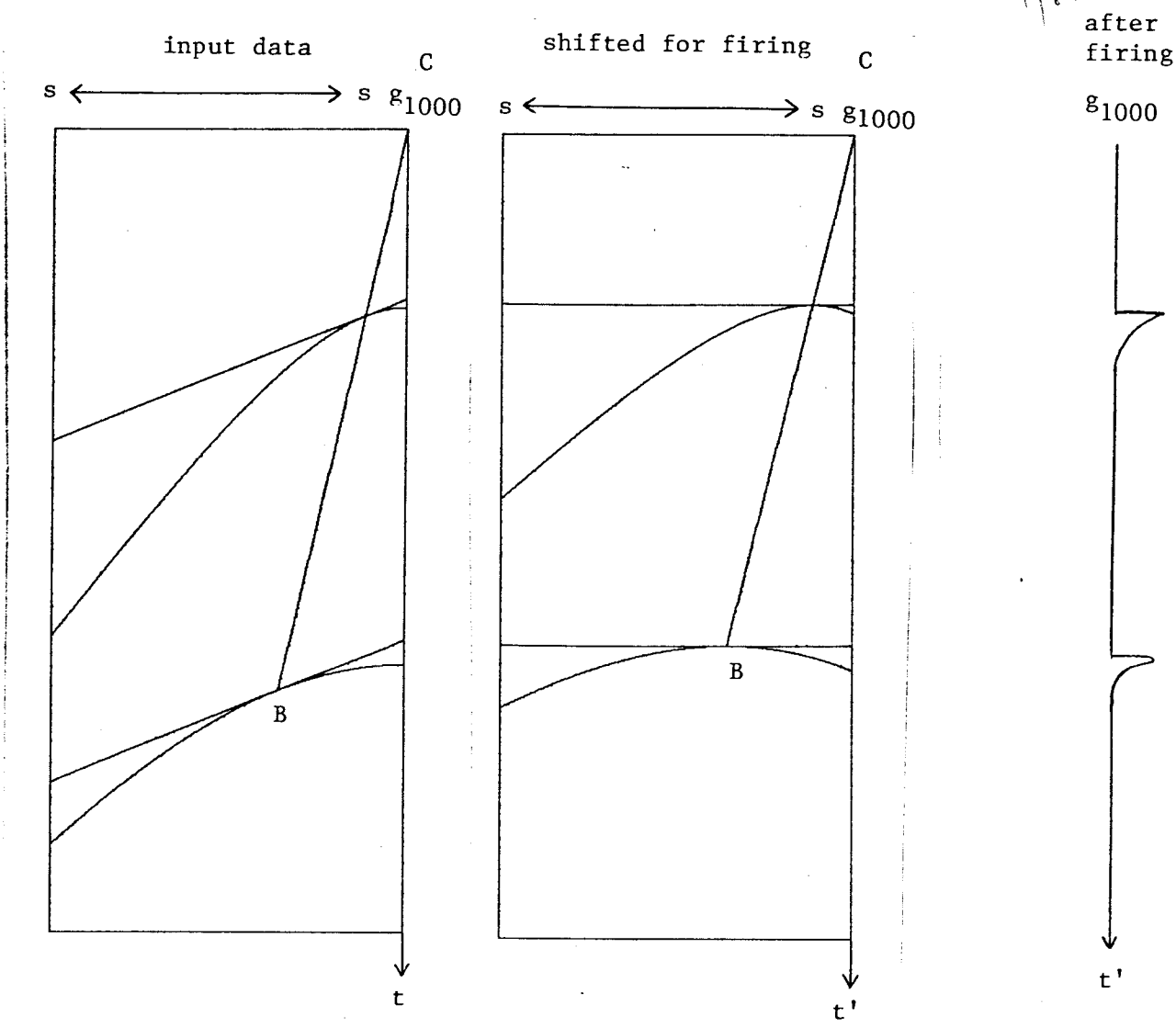

FIG. 5. Left shows a common geophone gather at g_{1000} over two flat reflectors. Center shows the data shifted by linear moveout in preparation for generation of the synthetic Snell wave by summation over shots. Right shows the Snell wave trace recorded at geophone g_{1000}. A seismic section for input to equation (19) consists of many side-by-side traces like g_{1000}.

For horizontal beds there is no detection of lateral location, unless we allow an abrupt lateral change in reflection coefficient. On figure 4 the information about the reflection strength at B is actually recorded rightward at C instead of being seen at A where it would be on conventional stack. Moving received data to an appropriate lateral location is thus an additional requirement for full interpretation.

Figure 6 shows the same two flat layers as figures 4 and 5, but additionally there are anamolous reflection coefficients at the points A, B, and C. Point A is directly above B. The path of the wave reflected at B leads directly to C and thence to g_{1000}. Subsequent frames show the diffraction hyperbolas associated with these three points. Notice that the pseudo-Snell waves reflecting from the flat layers step out at a rate p. Hyperbolas from the scatters A, B, and C come tangent to the Snell waves at points a, b, and c. Notice that b and c lie directly under g_{1000} because all are aligned by a raypath with Snell parameter p. The points A, B, and C locate the tops of the hyperbolas since the earliest arrival must be directly above the point scatterer, no matter what the incident wave field. Converting to the interpretation coordinate t' in the next frame offers the major advantage that arrivals from horizontal layers become horizontal. But the hyperboloids have become skewed. Limiting our attention to the arrivals with little stepout we see that our information about the anomalous reflection coefficients is found entirely in the vicinities of a, b, and c, which originally lay on hyperbola flanks. These points do not have the correct geometrical location, namely that of A, B, and C, until we laterally shift information to the left, say $g' = g - f(t')$. Then a lies above b. The correct amount of shift $f(t')$ is a subject relating to hyperbola breadth and hence to velocity analysis. It also seems that the skewed hyperboloids are tending to straighten out, but I have not checked to see if their asymptotes become symmetric.

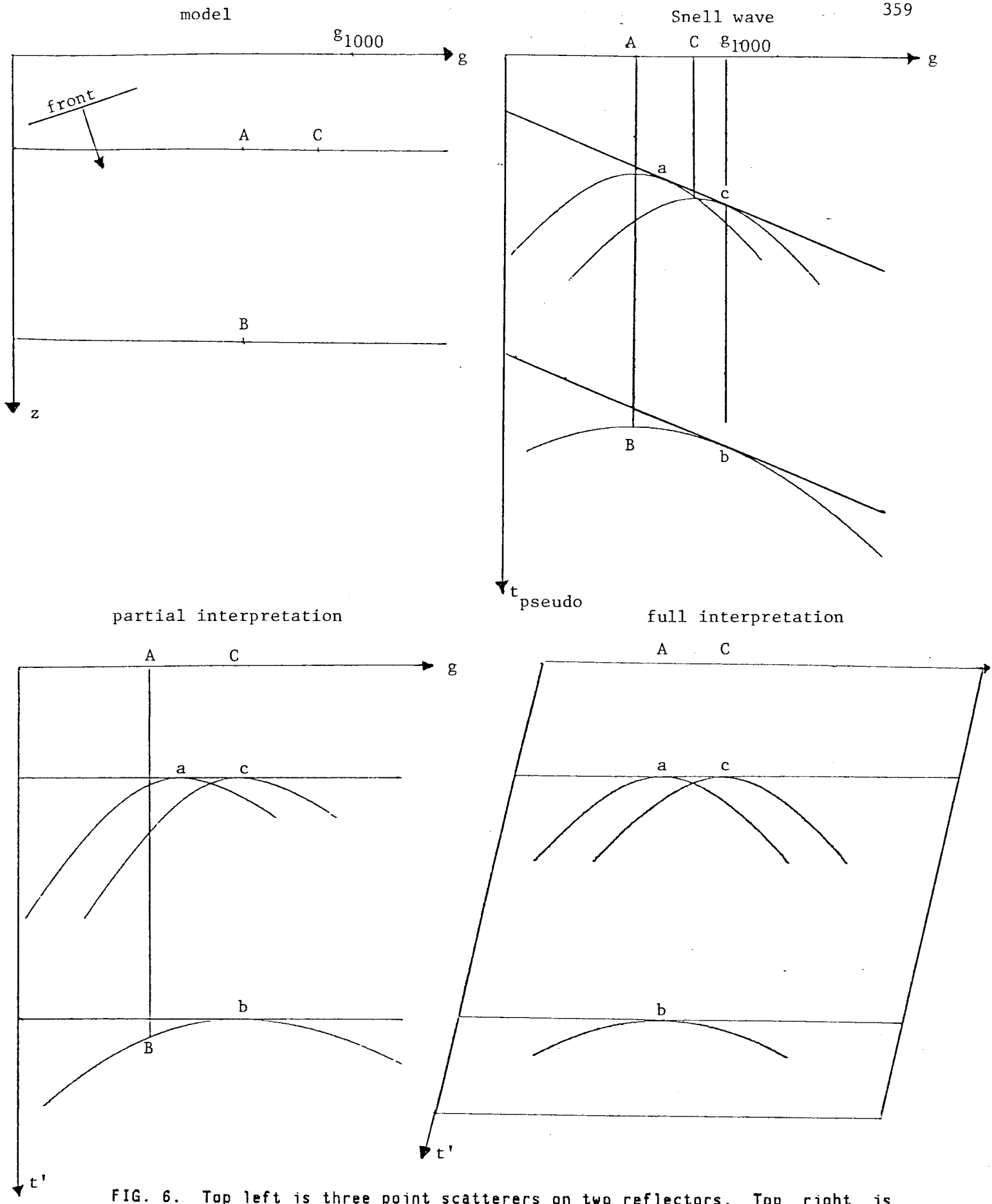

FIG. 6. Top left is three point scatterers on two reflectors. Top right is the expected Snell wave. Bottom left is the Snell wave after linear moveout. Bottom right is after transform to full interpretation coordinate. At last a, b, and c are located where A, B, and C began.